

# ILLUSTRATION NICKEL OXIDE NANO-PARTICLES: SYNTHESIS AND SPECTRAL INSPECTION OF FUNDAMENTAL INTERACTION WITH SUCROSE

Neeraj Kumar Sisodiya<sup>1</sup>, Shailesh Kumar Singh<sup>2</sup>

<sup>1</sup>Student M.Sc., Monad University

<sup>2</sup> Associate Professor K.K University Bihar

\*\*\*

**Abstract** - Nickel oxide (NiO) nanoparticles were with success synthesized by the reaction of nickel chloride with hydrazine at room temperature and thermal decomposition of the precursor nickel hydroxide (Ni(OH)<sub>2</sub>) nanoparticles. The production were characterized by X-ray diffraction, Transmission electron microscopy, Fourier transform infrared spectroscopy, and UV-vis assimilation spectroscopy. The result of thermogravimetric synthesis showed that the Ni(OH)<sub>2</sub> nanoparticles are calcinated at ~400 °C. The interactions between NiO nanoparticles and glucose have been designed using UV-vis assimilation and fluorescence spectroscopy. The zeta-potential of NiO nanoparticles was used to gain insight about the physical phenomenon mode between NiO nanoparticles and glucose.

**Key Words:** Nickel Nanoparticles, Glucose, Fluorescence

## 1. INTRODUCTION

This document is template. Trichomic films, and magnetic materials. It can also be extensively used in dye sensitized photocathodes. It exhibits anodic electrochromic, excellent permanency and electrochemical stability, large spin optical density and various manufacturing possibilities. Also for low material cost as an ion storage material, NiO semiconductor becomes a motivating topic in the new area of research. Because of the volume effect, the quantum size effect, the surface effect and the macroscopic quantum tunnel effect, nanocrystal line NiO is expected to possess many developed properties than those of micrometre-sized NiO molecule.

With advancements in all areas of industry and technology, the interest has been focused on nanoscale materials, which stems from the fact that new properties are required at this length scale and, equally important, that these properties change with their size and morphology. Thus, many methods have been attempted to prepare Nano sized nickel oxide, including nanoparticles, Nano rings, Nano sheets, and nanoribbons. However, there are only few biosensor applications. Li. Developed a novel aerometric glucose sensor based on NiO hollow Nano sphere. The NiO is suitable for electrostatic immobilization of proteins having low ionization potential because the ionization potential of NiO is about 10.7 eV

and the hollow-sphered NiO was good responsible for high loading of glucose oxidase and showed fast electron transfer with a sensitivity of 3.43  $\mu\text{A mM}^{-1}$  and a detection limit of 47  $\mu\text{M}$  (S/N=3). Fluorescence based glucose sensors have appeared in the literature as an alternative way of continuous monitoring of glucose levels. These sensors are highly specific towards analytes but require built-in probes. It has been reported that glucose is used as a reducing agent in chemical compound of metal nanoparticles. So it could be assumed that glucose in blood serum would affect the optical properties of NiO nanoparticles when they are used in the organism. In the last decade the use of glucose biosensor was manufacture by using metal nanoparticles and metal-oxide including zinc oxide, copper oxides, manganese dioxide, titanium oxides, cerium oxide and silicon dioxide.

In the existing work, we report the synthesis of NiO nanoparticles by the chemical reduction of nickel chloride with hydrazine at room temperature and thermal decomposition of the precursor nickel hydroxide nanoparticles. Also, the physical phenomenon between NiO nanoparticles and glucose have been obstinate using UV-vis absorption and fluorescence spectroscopy. The zeta-potential measurements are used to assess the physical phenomenon mode. Experimental outcome have demonstrated that the optical properties of glucose solution can be altered by the addition of nickel oxide nanoparticles. This finding is important for optical glucose sensors.

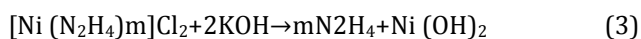
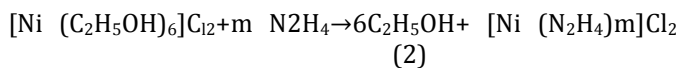
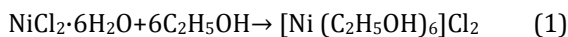
## Experimental

### 1.1 Materials

All chemicals used in this experiment were of reagent grade and used without any further purification. Nickel chloride hexahydrate (NiCl<sub>2</sub>·6H<sub>2</sub>O) was purchased from Wilkinson-Vickers Ltd., hydrazine monohydrate (N<sub>2</sub>H<sub>4</sub>·H<sub>2</sub>O) solution was purchased from Merck, potassium hydroxide (KOH) was purchased from Sigma-Aldrich. Ethyl alcohol and acetone were received from Merck. All solutions were prepared with deionized water.

## 1.2 Synthesis of nickel oxide nanoparticles

NiO nanoparticles were synthesized by thermal decomposition of Ni(OH)<sub>2</sub> by modification of the method reported by Gangway et al. Nickel chloride hexahydrate (0.111 M) in absolute ethanol were used as precursors, and were added to hydrazine monohydrate solution (6.73 ml of molar ratio 5). The pH was adjusted from 8.0 to 12 using potassium hydroxide. The reaction was stirred for 2 h at room temperature. The resultant product was washed thoroughly with deionized water for removal of reaction residues followed by washing with acetone. Finally, deep green nanoparticles [Ni(OH)<sub>2</sub>·0.5H<sub>2</sub>O] were formed, and dried in vacuum. The nickel hydroxide nanoparticles were converted to NiO via thermal decomposition at 600 °C. During the synthesis of NiO nanoparticles, the following reactions are reasonable to propose:



## 2. Equipment

UV-vis absorption spectra were measured on a Shimadzu UV-2450 spectrophotometer. Fluorescence spectra were recorded on a Shimadzu RF-5301PC spectrofluorometer. The Fourier-transform infrared (FT-IR) spectra were measured with a JASCO spectrometer 4100 using the KBr pellet technique. The X-ray diffraction (XRD) measurements were conducted by using a Shimadzu 6000-XRD X-ray diffractometer using CuK $\alpha$  radiation ( $\lambda=1.54056 \text{ \AA}$ ). Transmission electron micrographs (TEM) were obtained using a JEOL 2010 microscope operating at an accelerating voltage of 200 kV. Zeta potential results were carried out on Brookhaven zeta potential/particle size analyzer.

## 3. Spectral measurements

It should be emphasized that when the interaction of particles with glucose was conducted at constant concentration of NiO nanoparticles, the absorption and emission data show little spectral changes. However, considerable spectral changes were observed when the interactions of the nanoparticles with glucose were performed at different concentrations of NiO nanoparticles and constant glucose concentration. This was likely because the reactions occur on the surfaces of NiO nanoparticles. Increasing the surface area of nanoparticles generally increases the rate of chemical reactions. The pH

of the aqueous solutions was adjusted by phosphate buffer. All experiments were performed at pH 6.8, unless otherwise specified.

## 4. Results and discussions

### 4.1 Characterization of nanoparticles

In order to reveal the changes that occurred during heat treatment of the precursor powders, TGA analysis were carried out from 25 to 600 °C in atmosphere (Fig. 1). It is readily seen that the TGA curve showed two steps of weight loss. The first weight loss (found 8.6 wt%, Cal. 8.8 wt%) in a temperature range of 25–210 °C can be ascribed to the evaporation of half water molecule of crystallization. The second weight loss (found 17.8%, Cal. 17.7%) is due to the elimination of one water molecule in the range of 210–400 °C and associated with the thermal decomposition of Ni(OH)<sub>2</sub> to NiO nanoparticles. When temperature is above 400 °C, weight loss becomes fairly slight; indicating the formation of NiO nanoparticles is nearly complete. The TGA analysis verifies that the Ni(OH)<sub>2</sub> nanoparticles are calculated at 400 °C. Above 400 °C, obviously there is no change in the weight of the precursor in the TG curve as antecedently reported. The thermal decomposition processes of [Ni(OH)<sub>2</sub>·0.5H<sub>2</sub>O] can be represented as

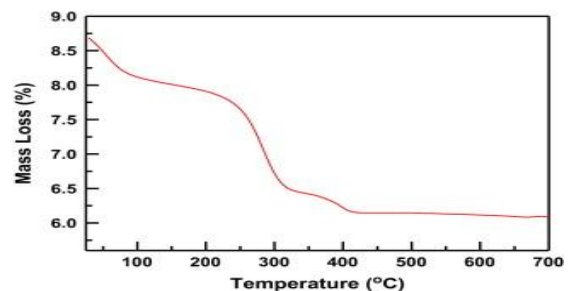
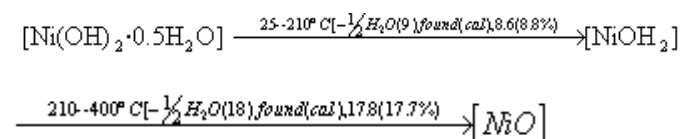


Fig. 1. TGA of Ni(OH)<sub>2</sub> nanoparticles.

The kinetic and thermodynamic parameters: enthalpy  $\Delta H$ , entropy  $\Delta S$ , Gibbs free energy  $\Delta G$  as well as activation energy  $\Delta E$  for decomposition of [Ni(OH)<sub>2</sub>·0.5H<sub>2</sub>O] were calculated from dynamic TGA by the use of Sharp-Wentworth and Freeman-Carroll methods and the results are shown in Table 1.

Sample	Step	T (K)	A	R	E(kj mol <sup>-1</sup> )	H (kj mol <sup>-1</sup> K <sup>-1</sup> )	S(kj mol <sup>-1</sup> )	G(kj mol <sup>-1</sup> )
[Ni(OH) <sub>2</sub> .1/2H <sub>2</sub> O] (101.7)	1st	411.6	2.84896	0.985	9.092	6.173	-0.224	-98.55
	2nd	573.3	7.93367	0.978	4.473	1.554	-0.184	-107.3

Table 1. The kinetic and activation thermodynamic parameters for decomposition of Ni(OH)<sub>2</sub>.

The values of these parameters are summarized in Table 1. The enthalpy change ΔH‡ is positive (endothermic) due to increase in adsorption on successive increase in temperature. Further, negative ΔG‡ values dictate spontaneous process at the reported temperature.

Fig. 2 shows the FT-IR spectra of the precursor Ni(OH)<sub>2</sub> and the oxide products NiO nanoparticles after calcination. A narrow and strong band at 3634 cm<sup>-1</sup> relating to the ν(OH) expansion vibration, which is the characteristic of Ni(OH)<sub>2</sub>. The broad and intense band centered at 3450 cm<sup>-1</sup> is assigned to the O-H stretching vibration of the interlayer water molecules and of the H-bound OH group. The peak observed at 1644 cm<sup>-1</sup> is assigned to the bending vibration of water molecules. The peaks observed at 1390 cm<sup>-1</sup>, 1300 cm<sup>-1</sup> and 1030 cm<sup>-1</sup> are respectively, assigned to the O-C=O symmetric and asymmetric stretching vibrations and the C-O stretching vibration originating from the adsorption of atmospheric CO<sub>2</sub> or ethanol, but the intensity of the band has weakened, which shows that the ultrafine powders tend to strong physically absorption to H<sub>2</sub>O and CO<sub>2</sub> Fig. 2. After calcination, the FT-IR spectra of NiO nanoparticles shows strong band at 425 cm<sup>-1</sup> corresponds to the vibration of Ni-O bond. It could be seen from Fig. 2 that the broad absorption band centered at 3450 cm<sup>-1</sup> is attributable to the band O-H stretching vibrations, due to the fact that the calcined powders tend to physically absorb water.

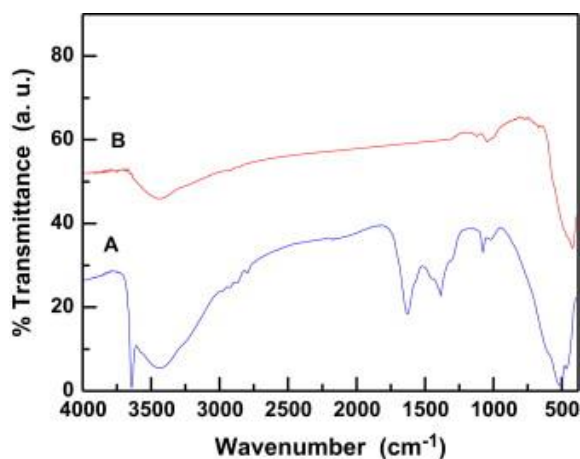


Fig. 2. FT-IR spectra of (A) precursor and (B) calcined powder.

Fig. 3(A and B) shows the XRD patterns of the precursor Ni(OH)<sub>2</sub> and NiO nanoparticles products after calcination. The peaks obtained for the hydroxide precursor seem to be appreciably broad which indicates that the crystallites of the hydroxide can be in the nano sized range. The difference in peak broadening to be related to crystallite shape, defects, and they differ in crystal symmetry, as well as crystallinity.

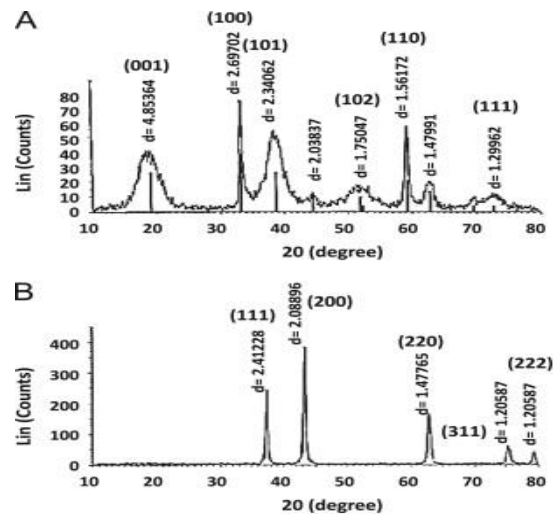


Fig. 3. XRD of the (A) precursor Ni (OH)<sub>2</sub> nanoparticles and (B) NiO nanoparticles.

The XRD patterns of the calcined sample exhibited sharpened reflection peaks which indicate that a growth in the crystallite sizes of NiO has occurred. The peaks positions appearing at 2θ=37.10°, 43.30°, 62.87°, 76.50°, and 79.22° crystal planes of the bulk NiO, respectively. All the reflections can be indexed to face-centered cubic (fcc) NiO phase with lattice constant (a): 4.175 Å (space group Fm3hm. which agrees well with the standard data (JCPDS card no. 47-1049). The sharpness and the intensity of the peaks indicate the well crystalline nature of the prepared sample. No peaks due to Ni(OH)<sub>2</sub> were found from XRD, indicating that Ni(OH)<sub>2</sub> was completely decomposed to NiO at 400 °C for 2 h, which is also confirmed by the TG measurement. The crystallite size based on X-ray peak broadening was estimated from the corresponding X-ray spectral peak employing the Debye-Scherer's formula (Eq. (6)).

$$D = k \lambda / \beta \cos \theta \tag{6}$$

Where k is an empirical constant equal to 0.9, λ is the wavelength of the X-ray source (1.5405 Å), β is the full width at half maximum of the diffraction peak and θ is the angular position of the peak. The crystallite sizes of NiO samples is 37.5 nm which was calculated from measured values for the spacing of the (111) plane.

The size and morphology of the nanoparticles were characterized by TEM. Typical TEM images of the Ni(OH)<sub>2</sub> and NiO nanoparticles are shown in Fig. 4(A and B). The TEM image of the precursor Ni(OH)<sub>2</sub>, clearly shows a uniform particles with a hexagonal shape having a diameter of about 45 nm. However, TEM image of NiO nanoparticles reveal a non-spherical particle shape with smooth and uniform particle morphology, Fig. 4B with average diameter (taken as average particle diameter) is nearly equal to 32 nm. We notice that the mean particle size determined by TEM values is in reasonable agreement with the average crystallite size calculated by Scherrer's equation from the XRD pattern.

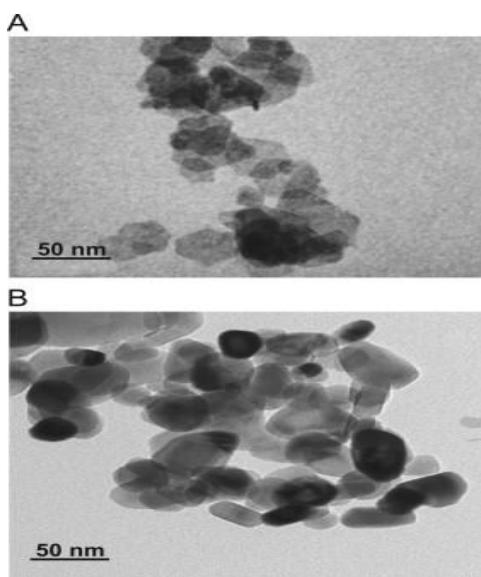


Fig. 4. TEM image of (A) precursor and (B) calcined powder.

$$\alpha h\nu = A(h\nu - E_g)^n \quad (7)$$

The absorption spectra of NiO nanoparticles are shown in Fig. 5. The energy band gap of these nanoparticles is estimated using the Tauc relation (7) where  $\alpha$  is absorption coefficient,  $h\nu$  is the photon energy,  $E_g$  is the band gap  $n=1/2$  for the direct transitions. A plot of  $(\alpha h\nu)^2$  versus  $h\nu$  is shown in the inset of Fig. 5 and the linear portion of the curve is extrapolated to  $h\nu$  axis to determine the band gap. The band gap is found to be 3.54 eV.

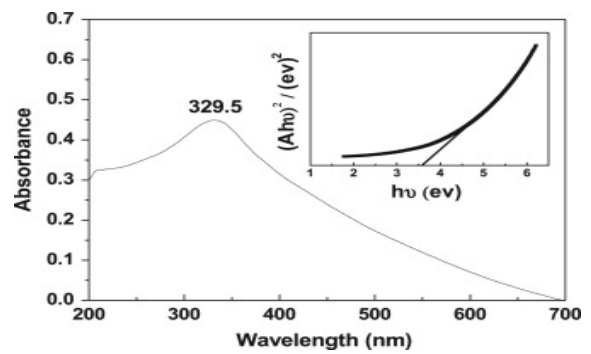


Fig. 5. UV-vis spectra of NiO nanoparticles.

Fig. 5 shows the UV-vis absorption spectra of NiO nanoparticles. The optical absorption peak intensity is found at ~330 nm (3.75 eV). From the curve the band gap of the NiO sample has been found to be ~3.54 eV, which is in agreement with value (3.55 eV) and close to the value (3.42 eV).

Fig. 6A shows the changes in the UV-vis spectra of the glucose upon interaction with different concentrations of NiO nanoparticles in aqueous solution of pH 6.8. It is apparent that, increasing the concentration of NiO nanoparticles from (0.5–7.5 × 10<sup>-4</sup> M) to glucose (1 × 10<sup>-4</sup> M) leads to a consistent increase of the glucose band at ~293 nm with a red shift to 327 nm. Fig. 6 B shows the calibration curve derived from the changes in the absorbance at  $\lambda=310$  nm as the concentration of NiO nanoparticles increases. The linear range scans the concentration of NiO nanoparticles from 0.5 to 7.5 × 10<sup>-4</sup> M with a correlation coefficient of 0.986. The results suggest an interaction between the nanoparticles and glucose.

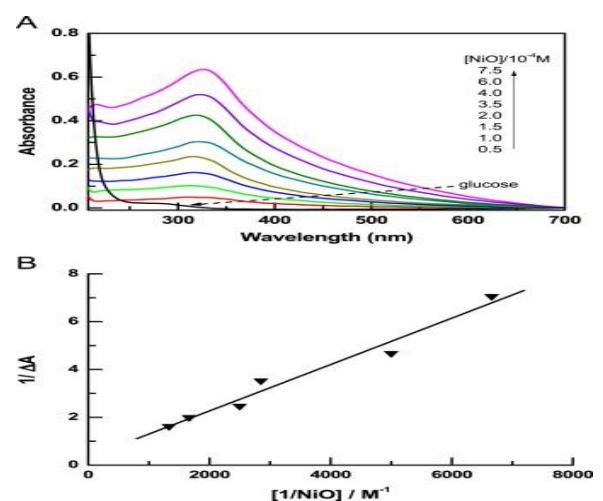


Fig. 6. (A) UV-vis absorption spectra of glucose (1 × 10<sup>-4</sup> M) in the absence and presence of NiO nanoparticles in buffer solution of pH 6.8 and (B) Benesi-Hildebrand plot for 1:1 glucose/NiO interaction.

The binding constant  $K$  and stoichiometric ratios of the interaction between glucose and NiO nanoparticles can be determined according to the double-reciprocal relations assuming the formation of a 1:1 host-guest complex.

$$\frac{1}{\Delta A} = \frac{1}{\Delta \epsilon} + \frac{1}{k[\text{glu cos } e]_0 \Delta \epsilon [\text{NiO}]} \quad (8)$$

where  $\Delta A$  is the difference between the absorbance of glucose in the presence and absence of NiO nanoparticles,  $\Delta \epsilon$  is the difference between the molar absorption coefficients of glucose and the complex.  $[\text{glucose}]_0$  and  $[\text{NiO}]_0$  are the initial concentration of glucose and NiO, respectively.

Fig. 6B depicts a plot of  $1/\Delta A$  as a function of  $1/[\text{NiO}]$  for glucose at various temperatures. Good linear correlations were obtained, consistent with the 1:1 interaction. From the intercept and slope values of this plot,  $K$  is evaluated. The observed value of the binding constant is  $3.4 \times 10^2 \text{ M}^{-1}$ .

To support the interaction between glucose and nanoparticles, we measured the luminescence spectra from solutions of the pure glucose and solutions of the glucose molecules with variable concentrations of NiO nanoparticles at an excitation wavelength of 273 nm, Fig. 7A. It is readily seen that the addition of  $7.5 \times 10^{-4} \text{ M}$  of NiO nanoparticles to  $1 \times 10^{-4} \text{ M}$  of glucose induced a strong fluorescence intensity enhancement at 360 nm up to 11-fold is observed, accompanied by a decrease in the fluorescence intensity at 303 nm. Thus is promising for the future development of glucose sensors.

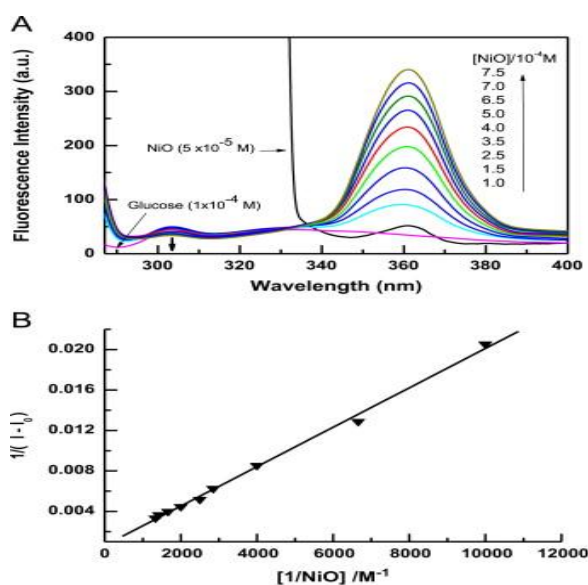
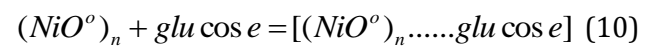


Fig. 7. (A) Fluorescence emission spectra of glucose ( $1 \times 10^{-4} \text{ M}$ ) in the absence and presence of NiO nanoparticles in buffer solution of pH 6.8.  $\lambda_{\text{ex}} = 273 \text{ nm}$ ; and

(B) Linear dependence of  $1/(I-I_0)$  on the reciprocal concentration of NiO nanoparticles.

Clean isosbestic points are observed at 330 nm, confirm the equilibrium between NiO nanoparticles and glucose. These results support the concept of the balanced interaction between NiO nanoparticles and glucose according to the following equation:



where  $[\text{NiO}]_0$  represents the initial concentration of NiO nanoparticles,  $I_0$  and  $I$  are the fluorescence intensities in the absence and presence of NiO, respectively and  $I_1$  is the limiting intensity of fluorescence.  $K$  is the association constants for 1:1 complex which can be calculated from the fluorescence data by Eq. (10). Fig. 7B displays a double-reciprocal plot for glucose with NiO nanoparticles. As can be seen, the plots are well described as single straight line, from which the values of binding constant has been determined. The calculated value at  $298 \text{ }^\circ\text{K}$  is equal to  $3.2 \times 10^2 \text{ M}^{-1}$ . The obtained  $K$  value is in reasonable agreement with that obtained from fluorescence spectral data within the experimental and curve fitting errors.

The zeta-potential is a function of the surface charge and is often used as an index of the magnitude of electrostatic interaction between NiO particles and is thus a useful measure of the interaction between NiO nanoparticles and glucose. Zeta potential of NiO nanoparticles was measured at  $\text{pH} = 5-8$ . The zeta-potential results show that particles are negatively charged, Fig. 8A.

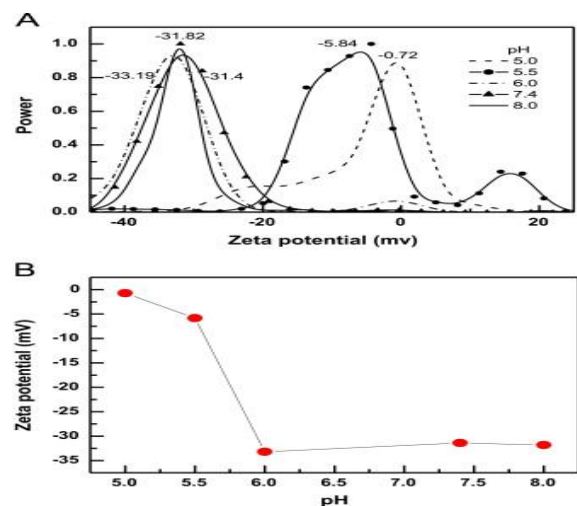


Fig. 8. (A) Zeta-potential of NiO nanoparticles in solutions of pH: 5 (---), 5.5 (-•-), 6.0 (-·-·-), 7.4 (-▲-) and 8 (—) and (B) the variation curve of Zeta potential as a function of pH value for NiO nanoparticles.

A plot of zeta potential of NiO versus pH (6.0–8.0) is shown in Fig. 8 B. It should be noted that the zeta potential versus pH curve is negative and the negative value increase with increasing pH value. However, from the plot, it is apparent that the sample is stable at pH values 6.0–8.0. Because of

negative charge, electrostatic repulsion forces exist between NiO and hydrophilic hydroxyl groups of glucose. Thus, the possible adsorption mode is that the hydrophobic part of glucose is adsorbed onto the surface layers of NiO by van der Waals interactions, and probably the hydrophilic part of the OH<sup>-</sup> is oriented toward the aqueous phase.

## 5. Conclusions

We have described an experimental procedure for the preparation of NiO nanoparticles based on chemical reduction of nickel chloride with hydrazine at room temperature and thermal decomposition of the precursor nickel hydroxide nanoparticles. The results obtained in this work provided some insights into the interaction between glucose and NiO nanoparticles. NiO nanoparticles have seriously affected the optical properties and stability of glucose and the possible interaction mode is that the hydrophobic part of glucose is adsorbed onto the surface layers of NiO by van der Waals interactions. Finally, one goal of this study is to motivate further biomedical applications of NiO nanoparticles.

## REFERENCES

- [1] K.M. Dooley, S.Y. Chen, J.R. Ross
- [2] *Journal of Catalysis*, 145 (1994), pp. 402-408 H.X. Yang, Q.F. Dong, X.H. Hu
- [3] *Journal of Power Sources*, 79 (1999), pp. 256-261. Hotový, J. Huran, L. Spiess, R. Čapkovic, Š. Haščík
- [4] *Vacuum*, 58 (2000), pp. 300-307 E.L. Miller, R.E. Rocheleau
- [5] Y. Ichiyanagi, N. Wakabayashi, J. Yamazaki, S. Yamada, Y. Kimishima, E. Komatsu, H. Tajima *Physica B*, 329-333 (2003), pp. 862-863
- [6] S.A. Makhlouf, F.T. Parker, F.E. Spada, A.E. Berkowitz
- [7] *Journal of Applied Physics*, 81 (1997), pp. 5561-5563 X.Y. Deng, Z. Chen *Materials Letters*, 58 (2004), pp. 276-290
- [8] S. Chakrabarty, K. Chatterjee *Journal of Physical Science*, 13 (2009), pp. 245-250
- [9] [10] J. He, H. Lindstrom, A. Hagfeldt, S.E. Lindquist *Journal of Physical Chemistry B*, 103 (1999), pp. 8940-8943
- [10] M. Ghosh, K. Biswas, A. Sundaresan, C.N. Rao J. Liang, Y.D. Li